PdeA is required for the rod shape morphology of Brucella abortus

Reboul, Angéline; Carlier, Elodie; Stubbe, François Xavier; Barbieux, Emeline; Demars, Aurore; Ong, Phuong Thi Anh; Gerodez, Antoine; Muraille, Eric; De Bolle, Xavier

Link to publication

Smart simplicity
IN ON-DEMAND TESTING

A simple and fast way to pinpoint patients most at risk with targeted and syndromic on-demand testing.

Our high multiplex technology is precision engineered for simplicity and accuracy across a broad and growing assay menu.

The Novodiag® System is part of our world leading Molecular Scalable Solutions, designed to effortlessly help you to meet the growing demands of your lab, today and in the future.

LEARN MORE

HOLOGIC®
NOVODIAG

PROF. XAVIER DE BOLLE (Orcid ID : 0000-0002-3845-3043)

Article type   : Research Article

PdeA is required for the rod shape morphology of *Brucella abortus*

Running Title: PdeA contributes to morphology of *B. abortus*

Angéline Reboul[1], Elodie Carlier[1], François-Xavier Stubbe[2], Émeline Barbieux[1], Aurore Demars[1], Phuong Thi Anh Ong[1], Antoine Gerodez[1], Eric Muraille[1,3], Xavier De Bolle[1,#]

[1]URBM, Narilis, University of Namur, Namur, Belgium

[2]URPHYM-GEMO, University of Namur, Namur, Belgium

[3]Laboratoire de Parasitologie, Université Libre de Bruxelles and ULB center for Research in Immunology (U-CRI), Gosselies, Belgium

[#]Address correspondence to Pr. Xavier De Bolle, xavier.debolle@unamur.be, Phone: +32 81 72 44 38

Abstract

Cyclic-di-GMP plays crucial roles in the cell cycle regulation of the α-*Proteobacterium Caulobacter crescentus*. Here we investigated its role in the α-*Proteobacterium Brucella abortus*, a zoonotic intracellular pathogen. Surprisingly, deletion of all predicted cyclic-di-GMP synthesizing or degrading enzymes did not drastically impair the growth of *B. abortus*, nor its ability to grow inside cell lines. As other Rhizobiales, *B. abortus* displays unipolar growth from the new cell pole generated by cell division. We found that the phosphodiesterase PdeA, the ortholog of the essential polar growth factor RgsP of the Rhizobiale *Sinorhizobium meliloti*, is required for rod shape integrity but is not essential for *B. abortus* growth. Indeed, the radius of the pole is increased by 31±1.7 % in a $\Delta pdeA$ mutant, generating a coccoid morphology. A mutation in the cyclic-di-GMP phosphodiesterase catalytic site of PdeA does not generate the coccoid morphology and the $\Delta pdeA$ mutant kept the ability to recruit markers of new and old poles. However, the presence of PdeA is required in an intra-nasal mouse model of infection. In conclusion, we propose that PdeA contributes to bacterial morphology and virulence in *B. abortus*, but it is not crucial for polarity and asymmetric growth.

Keywords

Introduction

Brucellaceae are facultative intracellular Gram-negative cocobacilli, belonging to the Rhizobiales order of α-Proteobacteria family. Members of the *Brucella* genus are responsible for a worldwide zoonosis known as brucellosis, with important consequences for health and economy. In animal livestock, the disease leads to abortion and sterility. Human brucellosis, mainly caused by *B. melitensis*, *B. suis*, *B. abortus*, and *B. canis*, is

characterized by an acute phase with periodic undulant fever. The illness can evolve to a chronic infection, which could also be associated with endocarditis or meningitis (Pappas *et al.*, 2005).

In vitro HeLa and macrophage cell infection by *B. abortus* follows a three-steps model in which bacteria are found in three successive types of vacuoles (Celli, 2019). In Hela cells and RAW264.7 macrophages-like cells, G1 phase bacteria ("new-born") enter the cells, reside in an endosomal *Brucella* containing vacuole (eBCV) but remain blocked in G1 during the first hours after invasion. *B. abortus* resumes growth before the eBCV reaches the replicative niche in the endoplasmic reticulum (rBCV) (Deghelt *et al.*, 2014). After extensive replication in the rBCV, bacteria are captured in autophagosome-like compartments forming an autophagic BCV (aBCV) (Celli, 2019).

One characteristic of *Brucellae* shared with Rhizobiales, is their asymmetric unipolar growth, as it occurs at one pole during elongation and at midcell during the cell division (Brown *et al.*, 2012). Recently, it has been shown that newly synthesized peptidoglycan (PG) and lipopolysaccharide are only inserted at one pole of the bacteria, named the growing pole (Vassen *et al.*, 2019). The growing pole is characterized by the presence of the protein AidB, which also localizes at the constriction site in divisional cells (Dotreppe *et al.*, 2011). Division leads to two new growing poles, one in each daughter cell, that will mature into old poles after elongation and the next division event. The maturation of the growing pole into an old pole correlates with the polar accumulation of the histidine kinase PdhS and the fumarase FumC (Hallez *et al.*, 2007, Mignolet *et al.*, 2010). However, the molecular mechanisms regulating cell morphology, cell polarity and polar growth of *B. abortus*, both *in vitro* and inside infected cells have not been described so far.

Over the last three decades, extensive studies have been conducted to decipher the role of bis-(3'-5')-cyclic dimeric guanosine monophosphate (cdG) in bacteria. Present in most of the known bacterial species, this second messenger has been shown to be involved in a number of biological processes, such as biofilm formation, transition from acute to chronic infection, motility and virulence (Jenal *et al.*, 2017). In some bacterial species, cdG also regulates cell cycle, growth and morphology (Fernandez *et al.*, 2020, Gupta *et al.*, 2016, Kaczmarczyk *et al.*, 2020, Lori *et al.*, 2015). The cdG is synthesized and degraded by diguanylate cyclases (DGC) and phosphodiesterases (PDE) respectively.

DGC include GGDEF domains, while PDE contain EAL or HD-GYP domains (Ryan *et al.*, 2006, Ryjenkov *et al.*, 2005, Schmidt *et al.*, 2005). Recently, the protein RgsP (PDE) has been identified as a key player of the polar growth of *Sinorhizobium meliloti* (Schaper *et al.*, 2018). Interestingly, the *Brucella* homologue, BpdA (also named PdeA) has been shown to be required for the virulence of *B. melitensis* 16M and *B. abortus* 2308 in a mouse model of infection, but also for the morphology of *B. melitensis* (Khan *et al.*, 2016, Petersen *et al.*, 2011). Except for these two pioneer studies, nothing is known about the conservation of cdG-metabolizing enzymes among *Brucellae* species and their role in the pathogen *B. abortus*. Interestingly, PdeA is a major actor of cell cycle regulation in the α-Proteobacterium *Caulobacter crescentus* (Abel *et al.*, 2011).

In this study, we show that cdG family enzymes are not fully conserved among *Brucella* and that this second messenger does not play a crucial role in *in vitro* conditions in *B. abortus*. We highlighted a role for the phosphodiesterase PdeA in the morphology and in the virulence of *B. abortus* in mice.

Results

B. abortus 2308 genome only encodes 7 putatively active cdG metabolizing enzymes

We first performed BLAST analyses on 14 *Brucella* genomes representative of the diversity of this genus (Wattam *et al.*, 2014). We also included the closest known derivative of *Brucella*'s ancestor, *Ochrobactrum anthropi* (Barquero-Calvo *et al.*, 2009, Teyssier *et al.*, 2005). As shown in Fig 1, all *Brucella* strains display 11 genes encoding DGC, PDE or dual proteins with both domains, with the exception of *B. abortus* 2308 that possess only 10 genes. Twenty genes encoding DGC or PDE have been identified in *O. anthropi*.

Sequence alignments revealed that several events of pseudogenization occurred in the evolution of the *Brucella* genus (Fig 1; empty symbol), likely leading to the inactivation of the encoded protein. Strikingly, we found out that BpdB (Bab1_0512), Bab2_0622, Bab2_0859 and Bab2_0228 (according to *B. abortus* 2308 coding sequences annotations) appear to be specific to *Brucellae.* This suggests that those four genes might have been acquired through horizontal transfer (or duplication and strong divergence) after the separation of *Brucella* and *Ochrobactrum* genus. Interestingly, three

of them are located on the second chromosome, which is thought to be a stabilized megaplasmid having a lower density of essential genes compared to the chromosome 1 (Deghelt *et al.*, 2014, Paulsen *et al.*, 2002, Sternon *et al.*, 2018). Moreover, only *pleD* and *bab2_0228* seem to remain intact among the *Brucella* genus analyzed here. Overall, it seems that these families of enzymes were subjected to intense rearrangements along the evolution within *Brucellae*, which contrasts with the high sequence identity shared by the different species of the *Brucella* genus (Verger *et al.*, 1985).

B. abortus 2308 exhibits most of the gene decay we could observe in the strains we examined here. Three proteins are either inactivated due to a nucleotide deletion resulting in a frameshift (*bab2_0255* and *bab2_0622*, Figs 1 and S1) or absent (Bmei_0929). Our *in-silico* analyses revealed 8 genes encoding putative cdG-metabolizing enzyme in *B. abortus* 2308. Four of them contain a GGDEF domain (DGC), Bab1_0441 *(*or CsgB), Bab2_0228, Bab2_0630 (or PleD) and Bab2_0966 (Fig S2). Two proteins have an EAL domain (PDE), Bab1_0512 (or BpdB) and Bab2_0859. Two proteins contain both GGDEF and EAL domain: Bab1_0220 and Bab1_0507 (or PdeA). We did not find any proteins containing a HD-GYP domain. Detailed investigation of the protein sequences showed that Bab2_0966 has a truncated GGDEF domain, suggesting that this protein is no longer an active DGC. PdeA presents several mutations in the DGC active site residues, with SSDQF instead of the GG(D/E)EF. That is a conserved feature among *Brucellae* and in *O. anthropi*. Bab1_0220 has a mutation in the active site residues EAL (EAF), which seems to be specific to *B. abortus* species (to the exception of *B. inopinata* in which the homolog of *bab1_0220* seems to be a pseudogene). Those results suggest that both PdeA and Bab1_0220 could actually be monofunctional in *B. abortus* 2308.

This *in silico* analysis suggests that *B. abortus* 2308 only encodes 4 DGC and 3 PDE, which contrasts with the 11 enzymes identified in *B. melitensis* 16M (Petersen *et al.*, 2011). These genes and predicted encoded proteins were also identified in *B. abortus* 544 with 100 % identity (data not shown).

cdG does not regulate *B. abortus in vitro* growth

To determine which role cdG might play in *B. abortus*, we generated single deletion mutants of each of the seven genes previously identified in *B. abortus* 544 wild type strain (WT). We assessed their ability to grow in rich (TSB) or defined medium (Plommet

Erythritol, PE) and in RAW264.7 macrophages-like cells. None of the mutants displayed a phenotype (Fig S3). As redundancy or compensatory activities of cdG metabolizing enzymes might explain the absence of strong phenotypes with single deletion mutants, we generated a quadruple mutant of the DGCs (Δ*csgB* Δ*pleD* Δ*bab1_0220* Δ*bab2_0228*, here referred as Δ4DGC), and a triple mutant of the PDEs (Δ*pdeA* Δ*bpdB* Δ*bab2_0859*, referred as Δ3PDE). While the Δ4DGC does not have a notable phenotype, the Δ3PDE mutant showed a minor growth defect in TSB (Fig S4, **, $p<0.05$, in a Mann and Whitney test).

We noticed that the Δ*pdeA* and Δ3PDE mutant strains formed small colonies, compared to the WT strain, after 4 days on TSB agar plates (Fig S5). Time course analyses revealed that these small colonies reach the same size as the WT strain colonies (Fig S5). In order to complement the phenotype, empty pMR10 was introduced in both the WT strain and the Δ*pdeA* mutant. We observed that the pMR10 vector slightly slows down the growth of the Δ*pdeA* mutant, both *in vitro* and in RAW264.7 cells but these defects were fully complemented when *pdeA* is inserted in the pMR10 (Fig S6). Complementation of the mutant strain with the pMR10 bearing *pdeA* restored bacterial growth to the WT level on plates (Figs 2A and S5).

Taken all together, those results suggest that cdG does not play a crucial role in *in vitro* growth, regardless of the medium, or in intracellular growth of *B. abortus* in a simple cellular infection model.

The phosphodiesterase PdeA modulates rod shape morphology of *B. abortus*

We next assessed if the disruption of each of these genes could impair the morphology of *B. abortus*. Only the *pdeA* mutant (Δ*pdeA*) displayed significant size modifications, with smaller and wider shape, adopting a coccoid almost spherical morphology (Figs 2B and S7, table S1A). Lengths and widths of the WT and Δ*pdeA* mutant, both bearing the empty pMR10 vector were measured to obtain the width to length (w/L) ratios. This analysis revealed that the Δ*pdeA* mutant was significantly rounder than the WT strain, with mean w/L ratio of 0.888 and 0.536, respectively (Fig 2C, $p < 0.0001$, in one-way analysis of variance). Deeper investigations of bacterial length and width showed that the Δ*pdeA* mutant was significantly shorter but also wider than the WT strain (Figs 2D-E and Fig S8A-B, table S1B). The Δ*pdeA* mutant displays an average length of 1.227 μm and an

average width of 1.058 μm compared to 1.521 μm and 0.805 μm for the WT strain, respectively ($p < 0.0001$ in a one-way ANOVA). Complementation of the mutant strain with the pMR10 bearing *pdeA* restored the wild type shape (length 1.513 μm; width 0.806 μm), showing that this alteration is indeed due to the loss of PdeA and not to polar effects or ectopic mutations. This morphology alteration was also observed in constricting bacteria (Fig S8C-E, $p < 0.0001$ in a one-way ANOVA). The wider shape of the bacteria implies that the size of the pole is strongly impaired in the $\Delta pdeA$ mutant. Indeed, measurements of the pole radius showed that the $\Delta pdeA$ mutant pole is 31 ± 1.7 % (mean ± SD) larger than the WT strain.

Deletion of the two other PDEs in the $\Delta pdeA$ strain did not worsen the morphological aspect of the strain (Fig S9, table S1C). The $\Delta4DGC$ mutant was morphologically identical to the WT strain. These results suggest that PdeA is required to maintain the integrity of the rod shape morphology.

PdeA does not rely on its phosphodiesterase activity to impact bacterial morphology

From our *in-silico* analyses, we showed that PdeA is likely a phosphodiesterase for cdG. Hence, the absence of this protein could potentially lead to an accumulation in cdG in bacterial cells. It has been previously shown that high levels of intracellular cdG might lead to small colony variant or alter the cell morphology (Gupta *et al.*, 2016, Starkey *et al.*, 2009). Therefore, we wanted to assess if the alterations of the $\Delta pdeA$ mutant colony size and morphology were due to an accumulation of cdG. We introduced a point mutation in the catalytic site of the EAL domain (PdeA^{E742A}) to abrogate its phosphodiesterase activity (Rao *et al.*, 2008). This mutation did not lead to a colony size defect (Figs 3A and S5). Interestingly, this mutation did not generate coccoid morphology either (Fig 3B-D, table S1D). These data suggest that the alteration of morphology in the $\Delta pdeA$ mutant is not due to the lack of phosphodiesterase activity of PdeA.

As the deletion of *pdeA* leads to a strong morphological defect independent of the phosphodiesterase activity, we wanted to reevaluate the role of the other phosphodiesterases on cell morphology. Hence, we also introduced the PdeA^{E742A} point mutation in a $\Delta bpdB$ $\Delta bab2\_0859$ double mutant strain, leading to a catalytically dead

triple mutant (referred as Δ*B59* PdeA[E742A]). This mutant did not display any colony size defect (data not shown) nor morphological defect (Figs 3E-G, table S1D). It is thus likely that morphological defects of the Δ*pdeA* mutant are not due to the absence of a cdG phosphodiesterase activity in this strain.

Lastly, evaluation of *in vitro* growth and in macrophages-like cells showed no difference between the WT strain and the two catalytically dead mutants (Fig S10). Overall, these results confirm that putative changes in cdG concentration do not seem to play a crucial role for the *in vitro* growth conditions tested here.

Asymmetric growth is maintained in the *pdeA* mutant

Considering the coccoid shape of the Δ*pdeA* mutant, we hypothesized that this loss of rod-shape morphology might be correlated with a perturbation of the polar (thus asymmetric) growth. To address this hypothesis, bacteria were labeled with the eFluor[670] dye (later named eFluor). eFluor binds to the accessible reactive amines on the bacterial surface. As the cells grow in absence of the dye, newly synthesized material that is incorporated at the growing pole of the cell are unlabeled, and since the outer membrane has a poor apparent fluidity, the unlabeled zone remains at the pole or at the division site (Vassen *et al.*, 2019). Hence, eFluor labeling allows to discriminate the labeled old pole from the unlabeled growing pole (Vassen *et al.*, 2019). As for the WT strain (Fig 4A eFluor and B, upper panels), an eFluor unlabeled region was observed at one pole of the bacterium in the Δ*pdeA* mutant (Fig 4A eFluor and B, bottom panel), revealing that despite its almost round morphology, the Δ*pdeA* mutant still exhibits asymmetric growth. As it can be tricky to correctly identify poles in an almost spherical bacteria, we took advantage of the eFluor labelling. This analysis allowed us to confirm that the Δ*pdeA* mutant is indeed shorter and wider than the WT strain (*p < 0.0001* in an unpaired t-test, data not shown).

Prior to microscopic observations, bacteria were short pulsed with the fluorescent D-amino acid HCC-amino-D-alanine (HADA) to follow the sites of synthesis and recycling of PG (Kuru *et al.*, 2012). In agreement with the previously described insertion sites (Vassen *et al.*, 2019), HADA was inserted at the new pole and at the constriction site in 84.5 % and 11 % of the WT bacteria, respectively (Figs 4A and C, upper panel, 4D). Interestingly, PG was also incorporated at the opposite pole of the eFluor labeling in the

Δ*pdeA* mutant (Fig 4A and C, bottom panel), consistent with the preservation of asymmetric growth in the absence of PdeA. However, analysis of the intensity of fluorescence indicated that the proportion of bacteria with a polar incorporation of HADA was significantly reduced to 57 % in the Δ*pdeA* cells but HADA incorporation is found at midcell (no visible sign of constriction) in 19 % of the bacteria (2 % for the WT strain) (Fig 4D, *p < 0.0001* in a two-way ANOVA). HADA incorporation was found at the constriction site in 19 % of the population of Δ*pdeA* mutant. These data show that the localization of HADA-labeled PG is perturbed in the absence of PdeA, since the sharp transition from polar to midcell signal clearly visible in the WT is replaced by a smooth transition and an extended polar localization to midcell in the Δ*pdeA* mutant. Moreover, the proportion of the cell surface labeled with HADA seems to be much more extended in the Δ*pdeA* mutant compared to the WT strain. Indeed, it appears from the microscopic observations and the demographic representation that HADA labeled the sidewalls of the growing zone of the cells in the mutant strain, while HADA labeling is concentrated at the tip of the pole in the WT strain (Fig 4C). In order to quantify this difference in the incorporation zone, we measured the HADA labeled area (quantified with ImageJ plug-in MicrobeJ (Ducret *et al.*, 2016)) in the WT and the mutant strains. There is no significant difference in the bacterial area between the WT and the mutant strains (Fig 4E). Hence, we calculated the percentage of HADA labeled area per bacterium. As this difference is mostly observed when HADA incorporation is polar, we only considered polarly labeled bacteria, regardless of the eFluor staining. In the WT strain, HADA-PG covers 11.5 ± 2 % (mean ± SD) of the cells area, versus 23 ± 3 % for the mutant strain (Fig 4F, *p < 0.01* in an unpaired t-test). Altogether, these results suggest that PdeA is not required for asymmetric growth but might be needed to focus the insertion of newly synthesized material at the growth tip. Moreover, this clearly raises the hypothesis that asymmetric growth might not be driven by the cell morphology or the size of the pole.

Considering the round shape of the *pdeA* mutant strain and the higher number of constricting bacterial that we observed with the HADA labeling, we performed time lapse experiment to measure the doubling time of bacteria. Even though there is a tendency of the mutant to grow slightly slower than the WT strain (table S2, movies S1-S3), this difference is not statistically significant.

PdeA does not trigger the localization of polar markers

As the pole size of Δ*pdeA* is disturbed, we wondered if this defect might impair the localization of the pole associated proteins PdhS, FumC and AidB. We first investigated if PdeA plays a role in the maturation of the growing pole into an old pole or in the localization of the old pole markers, through the analysis of PdhS and FumC. We labeled bacteria with eFluor in order to identify the old pole. PdhS-YFP and FumC-YFP localized at the eFluor labeled pole, both in the WT and the Δ*pdeA* strain (Figs 5A-B and S11). In rare cases, we detected PdhS-YFP or FumC-YFP at the growing pole or at midcell in the Δ*pdeA* mutant. However, these phenotypes were also observed in a few WT bacteria. Although there are statistically different recruitment patterns between the WT strain and the Δ*pdeA* mutant, the amplitude of these difference is small. This supports the hypothesis that, despite a strongly affected morphology, there is no major alteration of the old pole or of its maturation in the absence of PdeA.

We then analyzed the localization of AidB-YFP. In most exponentially growing cells, AidB-YFP localized at the growing pole and at the constriction site in elongated cells, regardless of the strain (Figs 5C and S11). In a few bacteria, we did observe AidB at the same pole as the eFluor labeling, what was never observed with the WT strain. AidB-YFP was found more often at the midcell and at the constriction site in the Δ*pdeA* mutant (Fig 5C, right panel), which is consistent with the higher number of constricting bacteria we observed with the PG labeling. However, we should be careful regarding the localization of AidB-YFP at the midcell. Indeed, the coccoid morphology might lead to a particular orientation on the pad and to a mis-interpretation in the localization of our protein of interest.

PdeA localizes at the growing pole and at the division site

We next aimed at localizing PdeA in the bacterial cell. To that end, we replaced the native *pdeA* with *pdeA-mCherry* at the chromosomal locus. This strain did not show a growth defect on plates, like the Δ*pdeA* strain, suggesting that the PdeA-mCherry fusion is at least partially functional. To determine its subcellular localization, we co-expressed PdeA-mCherry with the old pole marker PdhS-YFP (Hallez *et al.*, 2007). In most of the cells, PdeA-mCherry is either mainly found at the growing pole of the bacteria, opposite to PdhS-YFP, or at the constriction site (Figs 6A-C and S12). Quantitative analyses of the

fluorescence intensity showed that PdeA-mCherry localized at the growing pole in 80 % of the cells and at the constriction site in 8 % (Fig 6G).

As PdeA seemed to dynamically localize either at the growing pole or at the division site, we next assessed its localization compared to the growing pole-associated protein AidB. In 77 % of the cells, PdeA-mCherry was observed at the same pole as AidB-YFP (Fig 6D-F, 6H and Fig S12). It has also been observed at the constriction site together with AidB-YFP (7 %). In elongated cells where AidB-YFP is already relocated to the midcell or the constriction site, PdeA-mCherry was mainly found at the pole of the bacteria (7.6 %). These results strongly suggest that PdeA co-localizes at the growing pole with AidB and is then later redirected to the constriction site.

PdeA regulates the virulence of *B. abortus* in a mice model of infection

The homologs of PdeA in *B. melitensis* 16M and *B. abortus* 2308 have been previously shown to be required in a mouse model of infection through the intraperitoneal route (Petersen *et al.*, 2011). Here we assessed the role of PdeA in the virulence of *B. abortus* 544 in an intranasal model of infection in C54BL/6 mice that mimics the natural route of infection (Hanot Mambres *et al.*, 2016). We evaluated the capacity of the Δ*pdeA* mutant strain to colonize lung and spleen at 48 h, 5 days (d), 12 d and 28 d post infection. The Δ*pdeA* mutant failed to colonize the lungs as efficiently as the WT strain from the early times of infection (as soon as 48 h post infection), while the complemented strain is fully capable of multiplying in the lungs (Figs 7A and S13A). Deletion of *pdeA* also leads to a strong attenuation of *B. abortus* colonization of the spleen (Figs 7B and S13B).

Discussion

Bacterial genomes are in continuous evolution, sometimes allowing the emergence of pathogenicity. As demonstrated by Wattam *et al.*, *Brucellae* are no exception (Wattam *et al.*, 2014). In this study, we only identified seven (six in the case of *B. abortus*) cdG metabolizing enzymes in common with its closest known derivative ancestor, *O. anthropi* (that possess twenty putative enzymes, data not shown). We also identified four enzymes that are specific to *Brucellae*. Differences in the distribution of cdG signaling proteins in close relatives have been reported and likely relies on the adaptation of the organisms to its lifestyle (Galperin, 2005). As such, free living organisms possess more DGC/PDE proteins, among others signaling pathways, than do host adapted organisms or obligate

intracellular bacteria. For instance, several cdG encoding proteins were lost or inactivated during the evolution of *Y. pestis* from *Y. pseudotuberculosis*, which probably contributed to the adaptation of *Y. pestis* to the flea vector (Bobrov *et al.*, 2011, Hinnebusch & Erickson, 2008). Despite a very strong genetic homogeneity between *Brucellae* species, we spotted several pseudogenization events, even in the 4 genes that are specific to *Brucellae*. This actually is not so unexpected as small genomic variations such as pseudogenes occurrences have been shown to be associated with host preference (Suarez-Esquivel *et al.*, 2017, Suarez-Esquivel *et al.*, 2020, Tsolis *et al.*, 2009, Wattam *et al.*, 2009). As a host associated bacterium, *Brucellae* species might have evolved and selected mutations to ensure a tighter regulation of intracellular cdG concentration.

Our systematic approach to evaluate the role of PDE and DGC identified major differences regarding the role of cdG in *Brucellae* compared to what is known in other bacteria. We did not find any defect in growth or in host adaptation *in vitro*, with the exception of the putative encoded PDE PdeA. BpdA, the homologue of PdeA has been described as an active phosphodiesterase in *B. melitensis* (Khan *et al.*, 2016, Petersen *et al.*, 2011). Deletion of *pdeA* in both strains leads to common phenotypes, such as the alteration of the bacterial shape. Thus, we reasoned that PdeA is also an active phosphodiesterase in *B. abortus*, its deletion leading to an accumulation of cdG. The phenotypes we observed with the *pdeA* mutant strain correlate with previously described phenotypes associated with increased level of cdG. For instance, the mutant forms small colony on plates similarly to *P. aeruginosa* (Malone *et al.*, 2010, Starkey *et al.*, 2009). Alteration of the shape morphology is also a common characteristic of a high concentration of cdG (Fernandez *et al.*, 2020). As an example, in *Mycobacterium smegmatis*, which also exhibit polar growth but from both poles of the cells, high concentration of cdG reduces cell length (Gupta *et al.*, 2016). However, we clearly established here that none of the phenotype displayed by *B. abortus* Δ*pdeA* relies on its catalytic activity as catalytically inactive mutant exhibited normal growth and morphology. Surprisingly, strains lacking all predicted DGC or PDE were also not affected in any of the phenotypes we investigated here. Yet, we cannot exclude that *B. abortus* possess an undiscovered class of cdG metabolizing enzymes or that one of the genes we excluded in this study as a pseudogene actually encodes a functional DGC or PDE. Still, our

results are in accordance with the findings reported for *Sinorhizobium meliloti*, in which a strain devoid of cdG does not show drastic growth or morphological defects (Schaper *et al.*, 2016). In contrast, in the free-living bacterium *Caulobacter crescentus*, the phosphodiesterase PdeA, and the diguanylate cyclases PleD and DcgB control cell fate, asymmetric division and pole morphogenesis (Abel *et al.*, 2011, Abel *et al.*, 2013, Aldridge *et al.*, 2003, Duerig *et al.*, 2009, Kaczmarczyk *et al.*, 2020, Lori *et al.*, 2015, Paul *et al.*, 2004, Paul *et al.*, 2008). One might hypothesize that in the process of evolution and adaptation to a more restricted niche, cdG lost its role of regulator of cell cycle in favor of its role in virulence. This hypothesis might explain or be explained by the recent evolutional modifications of cdG metabolizing enzymes. Alternatively, it is also possible that the role of cdG as a cell cycle regulator is not ancestral in the α-Proteobacteria and could be specific to Caulobacteraceae.

We cannot exclude a more specific role of those enzymes in conditions we have not tested in this study. This is first supported by the differences between *in vitro* cell infection and mice infection we observed for the *pdeA* mutant, and secondly by the requirement of several enzymes to survive in bone marrow derived macrophages (Khan *et al.*, 2016). In many bacteria, cdG has been shown to be involved in the adaptation to stress conditions, i.e. in *S. meliloti* for acid stress response or in *L. pneumophila* to survive in poor-nutrients environments (Hughes *et al.*, 2019, Schaper *et al.*, 2016). In *E. coli*, the phosphodiesterase PdeC is maintained in its inactive form through the formation of a disulfide bond in its periplasmic loop, through the system DsbA/DsbB (Herbst *et al.*, 2018). In conditions of low oxygen supply, such as the deeper layers of a biofilm, a shift from oxidized PdeC to thiol-free state increases the phosphodiesterase activity of PdeC. Although Bab2_0859 only shares 32 % of identity with PdeC, it is interesting to note that, additionally to the conserved EAL domain and the periplasmic loop of about 200 amino acids flanked by two transmembrane domains, both the cysteines required for the formation of the disulfide bond are also conserved. As a human intracellular pathogen, *Brucellae* could face a low level of oxygen in the phagocytes and in deeper organs such as the spleen, liver and brain in some cases (Ariza *et al.*, 2001, Colmenero *et al.*, 2002, Colmenero Jde *et al.*, 2002, Sohn *et al.*, 2003).

As mentioned above, we provided evidence that PdeA is required to maintain a proper rod-shape of the bacteria but is strikingly less required than its ortholog in *S. meliloti* which is essential (Schaper *et al.*, 2018, Sternon *et al.*, 2018). This suggest that *B. abortus* could possess alternate mechanisms to ensure its polar growth which is surprising for a pathogen with a reduced genome. A decreased conjugation efficiency in the *pdeA* mutant prevents Tn-seq analyses to identify such a redundant molecular mechanism. Analyses of the *B. abortus* mutant also reveals that PdeA is required for the pole size and that recycling or incorporation of immature PG is slightly affected in the absence of PdeA. This is consistent with a role of PdeA in the recruitment of PG synthesis enzymes at the growing pole, as reported for RgsP in *S. meliloti*. Indeed, alteration in the composition and/or the localization of the PG synthesis and/or modification enzymes in the *pdeA* mutant could explain its aberrant morphology. As for the implication of RgsP in *S. meliloti* polar growth, PdeA displays the same localization as RgsP along the cell cycle, and all domains of *S. meliloti* RgsP are conserved in *B. abortus* PdeA. Similar to RgsP, the PDE function of PdeA is not required for pole size in *B. abortus*. The GGDEF domain of *S. meliloti* is required for polar growth (Schaper *et al.*, 2018). However, several mutations in this domain abrogate its ability to bind or synthesize cdG (Schaper *et al.*, 2018). This domain might also be important for the role of PdeA in *B. abortus.* Interestingly, degenerated GGDEF domain is conserved throughout the Rhizobiales homologs but this domain is intact in Caulobacteraceae. This could be an important feature in the evolution of micro-organisms and the discrepancies regarding the role of PdeA in *C. crescentus*, *S. meliloti* and *B. abortus*. RgsP control of the cell growth involves the proteins RgsM, a metallopeptidase and RgsA, an transmembrane protein but yet functionally and structurally uncharactized (Krol *et al.*, 2020). While a putative ortholog for RgsM is present in *B. abortus* (Bab1_1866, 52 % identity), we did not find such ortholog for RgsA. All these data suggest that PdeA could fulfill a similar role as RgsP, but in a different context, generating a difference in the phenotype of the corresponding mutants.

We showed here, that despite a coccoid morphology and an enlarged pole size, asymmetric growth is kept in the *pdeA* mutant. HADA is incorporated via enzymes such as the L,D-transpeptidases and this incorporation is not exclusively representative of the

incorporation of new PG in the envelope (Kuru *et al.*, 2019, Radkov *et al.*, 2018, Williams *et al.*, 2021). The extended HADA labeling that we observed in the absence of PdeA might also be due to cell wall remodeling.

We showed that the definition of the poles is conserved in the absence of PdeA. AidB recruitment to the growing pole is not affected, and further maturation in an old pole through the acquisition of PdhS and FumC still occurs like in WT strain. This suggest that the pole size is not a crucial determining factor in the fate of the bacterial pole. It is thus possible that polarity and asymmetric growth, which probably are intimately linked and evolutionary ancient, are resistant to genetic perturbations that impair pole morphology.

Such strong morphological defects could have been predicted to generate pleiotropic modification, leading to virulence attenuation. Surprisingly, the *pdeA* mutant is not affected in its ability to grow *in vitro* in RAW264.7 macrophages like cell line. However, our results showed that PdeA is required to efficiently colonize lungs and spleens in a mouse intranasal infection model, which is obviously much more complex than cells in culture and subjects *Brucella* to innate and adaptive immune defenses. This is in agreement with the results of Khan *et al*. and Petersen *et al*. who showed the involvement of the phosphodiesterase in the virulence of *B. melitensis* and *B. abortus* 2308 in a intraperitoneal infection model (Khan *et al.*, 2016, Petersen *et al.*, 2011). cdG has been involved in the regulation of virulence for several bacteria (reviewed in (Hall & Lee, 2018)), such as *Klebsiella pneumoniae* in which it attenuates virulence in lungs or *Pseudomonas aeruginosa* where it controls the transition from acute to chronic infection and vice versa, a feature shared by *Brucellae* (Galinska & Zagorski, 2013, Moscoso *et al.*, 2011, Rosen *et al.*, 2018). However, further characterizations are needed to confirm the role of the phosphodiesterase activity of PdeA in mice.

Experimental procedures

Ethic statement

The procedure used in this study and the handling of mice compliant with current European Legislation (Directive 86/609/EEC). The animal Welfare Committee of the

University of Namur (UNamur, Belgium) reviewed and approved the complete protocol for *B. abortus* infection (Permit Number: UN GIN 20/344).

Bioinformatics

Brucella assemblies (ASM18242v1, ASM15877v1, ASM74021v1, ASM5400v1, ASM1852v1, ASM18272v1, ASM712v1, ASM2274v1, ASM74225v1, ASM1684v1, ASM22100v1, ASM750v1, ASM15775v1, ASM1890v1) and *Ochrobactrum anthropi* assembly (ASM74295v1) were manually retrieved from NCBI. As the genome of *B. abortus* 544, our laboratory strain for biovar 1 of *B. abortus*, is not available in the NCBI data bank, we used the genome of *B. abortus* 2308 (also biovar 1), as a template. Cyclic di-GMP metabolizing enzymes were retrieved *via* annotation and BLAST-style alignment that queried for *Caulobacter crescentus* PleD (CCNA_02546; GGDEF domain), *Pseudomonas aeruginosa* PA2567 (EAL domain) and *Xanthomonas campestris* RpfG (XAACFBP6369_RS13410; HD-GYP domain) (Hecht & Newton, 1995, Kulasakara *et al.*, 2006, Ryan *et al.*, 2006). We validated our screen by comparing published *Brucella melitensis* 16M c-di-GMP enzymes to our list (Petersen *et al.*, 2011). Orthology relations were assessed by reciprocal best blast hit. Domains were aligned using MUSCLE (Edgar, 2004). Sequence polymorphism was manually screened. Domain identifications were performed with SMART (Schultz *et al.*, 1998).

Bacterial strains, plasmids and growth conditions

All strains, plasmids and sets of primers used in this study are listed in table S3. *Escherichia coli* DH10B (Invitrogen) and S17.1 (Simon *et al.*, 1983) were grown in Luria-Bertani (LB) medium at 37°C. *B. abortus* 544 (nalidixic acid resistant strain, referred as the WT strain) and its derivates were grown in tryptic soy liquid broth (TSB) at 37°C with shaking (160rpm). When required, antibiotics were added to the medium at the following concentrations, nalidixic acid, 25 μg mL^{-1}; kanamycin, 10 (integrative plasmid) or 50 (replicative plasmid) μg mL^{-1}; gentamycin, 10 or 50 μg mL^{-1}.

Deletion strains were constructed by double homologous recombination using the pNPTS138 vector and checked with polymerase chain reaction (PCR), as previously described (Deghelt *et al.*, 2014). Briefly, upstream and downstream regions of about 500 base pairs (bp) were PCR amplified for each gene of interest using the sets of primers listed in table S3. PCR products were joined by PCR overlap and cloned into the *EcoRV* site of the pNPTS138 vector. The resulting plasmids were introduced into *B. abortus* by

conjugation. Merodiploids were selected on kanamycin-nalidixic acid supplemented TSB agar plates, while excision of the plasmid was counterselected on 5 % sucrose TSB agar plates. The Δ*pdeA* mutant was complemented with the pMR10 vector containing the operon *bab1_0508-bab1_0507* (amplified with the primers set F-*PstI*-*pdeA* and R-*XhoI*-*pdeA*, listed in table S3) under the control of its own promoter (pMR10::*pdeA*).

Point mutation in the EAL active site of PdeA (E742A) was obtained by overlap PCR carrying the mutation with the primers listed in table S3 (catalytic mutant) and cloned into the *EcoRV* site of the pNPTS138. Double homologous recombination was applied to exchange the WT allele with the mutated one, as previously published (Deghelt *et al.*, 2014). Allelic replacement was checked by sequencing with primers that hybridize out of the homologous recombination zone.

When needed, the old pole markers PdhS-YFP (Hallez *et al.*, 2007), FumC-YFP (Mignolet *et al.*, 2010) and the growing pole marker AidB-YFP (Dotreppe *et al.*, 2011) (on pSK-integrative plasmid, Kan[R]) were integrated into the genome through a single homologous recombination.

The analyses of colony size were assessed by awakening strains from frozen stocks (-80°C) onto TSB agar plates (with Kanamycin when needed). Plates were incubated at 37°C and images after 3, 4 and 7 days. Assessment of growth was performed in TSB medium or in the chemically modified Plommet medium with erythritol as the sole carbon source (PE) (Barbier *et al.*, 2014). Overnight (O/N) culture were diluted to an optical density (OD_{600}) of 0.05 (TSB) or 0.1 (PE), 200µl were subsequently inoculated in flat bottom 96 well plates (Eppendorf) and grown for 48h at 37°C. OD_{600} was measured every 30min (with shaking prior to each measure) using an Epoch2 (Bioscreen).

Cell culture, infection and intracellular survival

RAW264.7 mouse macrophage-like cells were cultured at 37°C with 5 % CO_2 in DMEM Glutamax[TM] (Thermofisher scientific) supplemented with 10 % fetal bovine serum (Gibco). 5.10^4 cells were seeded into 24-well plates (Greiner® Bio-One) and infected at a multiplicity of infection of 50. When needed, antibiotic was added to the bacterial suspension prior to infection and kept during the infection. Infected cells were centrifuged for 10 min at 200 *g* at RT. After 1 hour of contact at 37°C with 5 % CO_2, medium was replaced with DMEM Glutamax[TM] supplemented with 50 µg mL^{-1} of gentamycin to kill remaining extracellular bacteria. Medium was changed after 1 h to DMEM Glutamax[TM]

containing 10 μg mL^{-1} of gentamycin. At different times post infection, the medium was removed; cells were washed two times with PBS and lysed with Triton X-100 (0.1 %) in PSB for 10 min at RT. Intracellular survival and growth were assessed by colony forming unit (CFU) counting on TSB agar plates.

Fluorescence microscopy

Bacteria were observed on PBS-1 % agarose pad (if not otherwise stated) with an inverted microscope Nikon Eclipse Ti2 (oil objective 100x, CFI plan Apo Lambda DM 100XH 1.45/0.13 mm) with the filter sets: Cy5.5B (eFluor, ex 655/40, DM 685, BA716/40); CFP-2432C (HADA, ex 438/24, DM 458, BA483/32); YFP-2427B (ex 500/24, DM 520, BA542/27); TxRed-4040C (mCherry, ex 562/40, DM 593, BA624/40). Pictures were acquired with an Orca Flash 4.0 V3 (Hamamatsu). All images were analyzed with ImageJ the plug-in MicrobeJ (Ducret *et al.*, 2016, Schneider *et al.*, 2012). Detailed procedures are provided in supplementary methods.

For microscopic observations and morphology quantification, bacteria were grown O/N in TSB, diluted into fresh TSB to an OD$_{600}$ of 0.1 and grown until early exponential phase was reached (OD$_{600}$ between 0.3 and 0.5). Two μl of culture were mounted on TSB agar pads and imaged. At least 300 bacteria from minimum three different fields were analyzed per pad. Only individual bacteria have been considered, divisional cells with a visible septum were manually selected and analyzed separately. Length and width of bacteria were determined and measured with the ImageJ plug-in MicrobeJ. For the statistical analyses, we calculated the median length and width for each experiment and we performed statistics on the mean of these three medians. For the pole radius measurement, we divided individual bacteria mean width by two to get the radius, calculated the median for each of the three replicates and the percentage of augmentation on the medians with the formula: ((Radius mutant – Radius WT) / Radius WT) *100. To measure the doubling time (i.e. the time period between two consecutive divisions), exponentially grown bacteria were labelled with eFluor and mounted on TSB agar pad. Bacteria were imaged every 20 minutes to produce time lapse movies. At least 6 bacteria were considered per experiment.

eFluor staining, peptidoglycan labeling and localization of polar proteins

To assess unipolar growth, O/N cultures were diluted to an $OD_{60 0}$ of 0.2, stained with eBioscience™ Cell Proliferation Dye eFluor™ 670 (eFluor, Invitrogen) to a final concentration of 5 µM in phosphate-buffered saline (PBS) for 15 min at RT, washed twice in PBS and incubated at 37°C with shaking in TSB (Vassen *et al.*, 2019). Bacteria were short-pulsed with HADA for 5 minutes at room temperature to a final concentration of 500 µM in TSB (Kuru *et al.*, 2012). Cells were fixed in ethanol for 15 minutes in 70 % ice cold ethanol on ice. Bacteria were imaged at the beginning of the experiment and in exponential phase (5-6 hours of growth). eFluor fully labeled bacteria were manually excluded as they cannot be oriented. To assess the localization of the PG incorporation or the polar proteins, only bacteria with a polar signal for eFluor have been taken into consideration in order to properly orient the bacteria. To quantify the HADA labeled area, we used the ImageJ plug-in MicrobeJ to detect the HADA area. Bacteria were manually checked and false maxima were excluded.

Localization of PdeA-mCherry

To localize PdeA in live bacterial cells, we replace the *pdeA* wild type gene with a *pdeA-mCherry* gene fusion, by double homologous recombination. Around 500bp of the 3' part of the gene (excluding the last 3 codons) and around 500bp of the 3' portion of the gene (including the last 13 codons, bearing a putative proteolysis tag) were amplified. *mCherry* gene was amplified from the pUC19::*mCherry* (F. Renzi, UNamur). All three fragments were joined by overlap PCR and cloned into the *EcoRV* site of the pNPTS138. Double homologous recombination was applied to exchange the WT allele with the mCherry fusion one. Allelic replacement was checked by PCR. O/N cultures were diluted to an OD_{600} of 0.2 and imaged in exponential phase of growth. Bacteria were manually selected in the smallest cell aggregated when possible. Only bacteria with one signal for PdhS-YFP or 1 or 2 signal(s) for AidB-YFP and at least one signal for PdeA-mCherry have been considered.

Mice infection

C57BL/6 mice were acquired from Harlan (Envigo, Bicester, UK). Eight 10-weeks female mice per group were infected intranasally with 30µl of a 6.6×10^5 CFU/mL (infectious dose: 2×10^4 CFU) in Prior to infection, mice were anesthetized with a mix of Xylasine / Ketamin (9mg/kg, 36mg/kg, respectively). The doses of infection were checked by plating serial dilutions on TSB agar plates. At desired time point, mice were sacrificed by cervical

dislocation. Spleen and lungs were immediately recovered and crushed in PSB 0.1 % Triton X-100 (Sigma Aldrich). We performed the experiment with and without (data not shown) the empty vector pMR10 in the WT and the Δ*pdeA* strains. Bacterial burden was evaluated by plating serial dilutions on TSB agar plates containing nalidixic acid and kanamycin (only for the experiment in which strains bear the pMR10. All experiments were handled in a Biosafety level 3 facility.

Data availability

All data supporting this study results are provided within the article and its supplementary information files or from the corresponding author upon request.

Acknowledgments

Author contributions

AR and XDB designed the work. AR and FXS performed the *in silico* analyses. AR, EC, PTAO and AG performed the *in vitro* experiments. AR, EB and AD did the *in vivo* experiments. EM provided tools and skills for the *in vivo* experiments. AR and XDB wrote the manuscript.

References

Abel, S., Bucher, T., Nicollier, M., Hug, I., Kaever, V., Abel Zur Wiesch, P., and Jenal, U. (2013) Bi-modal distribution of the second messenger c-di-GMP controls cell fate and asymmetry during the caulobacter cell cycle. *PLoS Genet* **9**: e1003744.

Abel, S., Chien, P., Wassmann, P., Schirmer, T., Kaever, V., Laub, M.T., Baker, T.A., and Jenal, U. (2011) Regulatory cohesion of cell cycle and cell differentiation through

interlinked phosphorylation and second messenger networks. *Mol Cell* **43**: 550-560.

Aldridge, P., Paul, R., Goymer, P., Rainey, P., and Jenal, U. (2003) Role of the GGDEF regulator PleD in polar development of Caulobacter crescentus. *Mol Microbiol* **47**: 1695-1708.

Ariza, J., Pigrau, C., Canas, C., Marron, A., Martinez, F., Almirante, B., Corredoira, J.M., Casanova, A., Fabregat, J., and Pahissa, A. (2001) Current understanding and management of chronic hepatosplenic suppurative brucellosis. *Clin Infect Dis* **32**: 1024-1033.

Barbier, T., Collard, F., Zuniga-Ripa, A., Moriyon, I., Godard, T., Becker, J., Wittmann, C., Van Schaftingen, E., and Letesson, J.J. (2014) Erythritol feeds the pentose phosphate pathway via three new isomerases leading to D-erythrose-4-phosphate in Brucella. *Proc Natl Acad Sci U S A* **111**: 17815-17820.

Barquero-Calvo, E., Conde-Alvarez, R., Chacon-Diaz, C., Quesada-Lobo, L., Martirosyan, A., Guzman-Verri, C., Iriarte, M., Mancek-Keber, M., Jerala, R., Gorvel, J.P., Moriyon, I., Moreno, E., and Chaves-Olarte, E. (2009) The differential interaction of Brucella and ochrobactrum with innate immunity reveals traits related to the evolution of stealthy pathogens. *PLoS One* **4**: e5893.

Bobrov, A.G., Kirillina, O., Ryjenkov, D.A., Waters, C.M., Price, P.A., Fetherston, J.D., Mack, D., Goldman, W.E., Gomelsky, M., and Perry, R.D. (2011) Systematic analysis of cyclic di-GMP signalling enzymes and their role in biofilm formation and virulence in Yersinia pestis. *Mol Microbiol* **79**: 533-551.

Brown, P.J., de Pedro, M.A., Kysela, D.T., Van der Henst, C., Kim, J., De Bolle, X., Fuqua, C., and Brun, Y.V. (2012) Polar growth in the Alphaproteobacterial order Rhizobiales. *Proc Natl Acad Sci U S A* **109**: 1697-1701.

Celli, J. (2019) The Intracellular Life Cycle of Brucella spp. *Microbiol Spectr* **7**.

Colmenero, J.D., Suarez-Munoz, M.A., Queipo-Ortuno, M.I., Reguera, J.M., and Morata, P. (2002) Late reactivation of calcified granuloma in a patient with chronic suppurative brucellosis. *Eur J Clin Microbiol Infect Dis* **21**: 897-899.

Colmenero Jde, D., Queipo-Ortuno, M.I., Maria Reguera, J., Angel Suarez-Munoz, M., Martin-Carballino, S., and Morata, P. (2002) Chronic hepatosplenic abscesses in

Brucellosis. Clinico-therapeutic features and molecular diagnostic approach. *Diagn Microbiol Infect Dis* **42**: 159-167.

Deghelt, M., Mullier, C., Sternon, J.F., Francis, N., Laloux, G., Dotreppe, D., Van der Henst, C., Jacobs-Wagner, C., Letesson, J.J., and De Bolle, X. (2014) G1-arrested newborn cells are the predominant infectious form of the pathogen Brucella abortus. *Nat Commun* **5**: 4366.

Dotreppe, D., Mullier, C., Letesson, J.J., and De Bolle, X. (2011) The alkylation response protein AidB is localized at the new poles and constriction sites in Brucella abortus. *BMC Microbiol* **11**: 257.

Ducret, A., Quardokus, E.M., and Brun, Y.V. (2016) MicrobeJ, a tool for high throughput bacterial cell detection and quantitative analysis. *Nat Microbiol* **1**: 16077.

Duerig, A., Abel, S., Folcher, M., Nicollier, M., Schwede, T., Amiot, N., Giese, B., and Jenal, U. (2009) Second messenger-mediated spatiotemporal control of protein degradation regulates bacterial cell cycle progression. *Genes Dev* **23**: 93-104.

Edgar, R.C. (2004) MUSCLE: multiple sequence alignment with high accuracy and high throughput. *Nucleic Acids Res* **32**: 1792-1797.

Fernandez, N.L., Hsueh, B.Y., Nhu, N.T.Q., Franklin, J.L., Dufour, Y.S., and Waters, C.M. (2020) Vibrio cholerae adapts to sessile and motile lifestyles by cyclic di-GMP regulation of cell shape. *Proc Natl Acad Sci U S A* **117**: 29046-29054.

Galinska, E.M., and Zagorski, J. (2013) Brucellosis in humans--etiology, diagnostics, clinical forms. *Ann Agric Environ Med* **20**: 233-238.

Galperin, M.Y. (2005) A census of membrane-bound and intracellular signal transduction proteins in bacteria: bacterial IQ, extroverts and introverts. *BMC Microbiol* **5**: 35.

Gupta, K.R., Baloni, P., Indi, S.S., and Chatterji, D. (2016) Regulation of Growth, Cell Shape, Cell Division, and Gene Expression by Second Messengers (p)ppGpp and Cyclic Di-GMP in Mycobacterium smegmatis. *J Bacteriol* **198**: 1414-1422.

Hall, C.L., and Lee, V.T. (2018) Cyclic-di-GMP regulation of virulence in bacterial pathogens. *Wiley Interdiscip Rev RNA* **9**.

Hallez, R., Mignolet, J., Van Mullem, V., Wery, M., Vandenhaute, J., Letesson, J.J., Jacobs-Wagner, C., and De Bolle, X. (2007) The asymmetric distribution of the essential histidine kinase PdhS indicates a differentiation event in Brucella abortus. *EMBO J* **26**: 1444-1455.

Hanot Mambres, D., Machelart, A., Potemberg, G., De Trez, C., Ryffel, B., Letesson, J.J., and Muraille, E. (2016) Identification of Immune Effectors Essential to the Control of Primary and Secondary Intranasal Infection with Brucella melitensis in Mice. *J Immunol* **196**: 3780-3793.

Hecht, G.B., and Newton, A. (1995) Identification of a novel response regulator required for the swarmer-to-stalked-cell transition in Caulobacter crescentus. *J Bacteriol* **177**: 6223-6229.

Herbst, S., Lorkowski, M., Sarenko, O., Nguyen, T.K.L., Jaenicke, T., and Hengge, R. (2018) Transmembrane redox control and proteolysis of PdeC, a novel type of c-di-GMP phosphodiesterase. *EMBO J* **37**.

Hinnebusch, B.J., and Erickson, D.L. (2008) Yersinia pestis biofilm in the flea vector and its role in the transmission of plague. *Curr Top Microbiol Immunol* **322**: 229-248.

Hughes, E.D., Byrne, B.G., and Swanson, M.S. (2019) A Two-Component System That Modulates Cyclic di-GMP Metabolism Promotes Legionella pneumophila Differentiation and Viability in Low-Nutrient Conditions. *J Bacteriol* **201**.

Jenal, U., Reinders, A., and Lori, C. (2017) Cyclic di-GMP: second messenger extraordinaire. *Nat Rev Microbiol* **15**: 271-284.

Kaczmarczyk, A., Hempel, A.M., von Arx, C., Bohm, R., Dubey, B.N., Nesper, J., Schirmer, T., Hiller, S., and Jenal, U. (2020) Precise timing of transcription by c-di-GMP coordinates cell cycle and morphogenesis in Caulobacter. *Nat Commun* **11**: 816.

Khan, M., Harms, J.S., Marim, F.M., Armon, L., Hall, C.L., Liu, Y.P., Banai, M., Oliveira, S.C., Splitter, G.A., and Smith, J.A. (2016) The Bacterial Second Messenger Cyclic di-GMP Regulates Brucella Pathogenesis and Leads to Altered Host Immune Response. *Infect Immun* **84**: 3458-3470.

Krol, E., Yau, H.C.L., Lechner, M., Schaper, S., Bange, G., Vollmer, W., and Becker, A. (2020) Tol-Pal System and Rgs Proteins Interact to Promote Unipolar Growth and Cell Division in Sinorhizobium meliloti. *mBio* **11**.

Kulasakara, H., Lee, V., Brencic, A., Liberati, N., Urbach, J., Miyata, S., Lee, D.G., Neely, A.N., Hyodo, M., Hayakawa, Y., Ausubel, F.M., and Lory, S. (2006) Analysis of Pseudomonas aeruginosa diguanylate cyclases and phosphodiesterases reveals

a role for bis-(3'-5')-cyclic-GMP in virulence. *Proc Natl Acad Sci U S A* **103**: 2839-2844.

Kuru, E., Hughes, H.V., Brown, P.J., Hall, E., Tekkam, S., Cava, F., de Pedro, M.A., Brun, Y.V., and VanNieuwenhze, M.S. (2012) In Situ probing of newly synthesized peptidoglycan in live bacteria with fluorescent D-amino acids. *Angew Chem Int Ed Engl* **51**: 12519-12523.

Kuru, E., Radkov, A., Meng, X., Egan, A., Alvarez, L., Dowson, A., Booher, G., Breukink, E., Roper, D.I., Cava, F., Vollmer, W., Brun, Y., and VanNieuwenhze, M.S. (2019) Mechanisms of Incorporation for D-Amino Acid Probes That Target Peptidoglycan Biosynthesis. *ACS Chem Biol* **14**: 2745-2756.

Lori, C., Ozaki, S., Steiner, S., Bohm, R., Abel, S., Dubey, B.N., Schirmer, T., Hiller, S., and Jenal, U. (2015) Cyclic di-GMP acts as a cell cycle oscillator to drive chromosome replication. *Nature* **523**: 236-239.

Malone, J.G., Jaeger, T., Spangler, C., Ritz, D., Spang, A., Arrieumerlou, C., Kaever, V., Landmann, R., and Jenal, U. (2010) YfiBNR mediates cyclic di-GMP dependent small colony variant formation and persistence in Pseudomonas aeruginosa. *PLoS Pathog* **6**: e1000804.

Mignolet, J., Van der Henst, C., Nicolas, C., Deghelt, M., Dotreppe, D., Letesson, J.J., and De Bolle, X. (2010) PdhS, an old-pole-localized histidine kinase, recruits the fumarase FumC in Brucella abortus. *J Bacteriol* **192**: 3235-3239.

Moscoso, J.A., Mikkelsen, H., Heeb, S., Williams, P., and Filloux, A. (2011) The Pseudomonas aeruginosa sensor RetS switches type III and type VI secretion via c-di-GMP signalling. *Environ Microbiol* **13**: 3128-3138.

Pappas, G., Akritidis, N., Bosilkovski, M., and Tsianos, E. (2005) Brucellosis. *N Engl J Med* **352**: 2325-2336.

Paul, R., Jaeger, T., Abel, S., Wiederkehr, I., Folcher, M., Biondi, E.G., Laub, M.T., and Jenal, U. (2008) Allosteric regulation of histidine kinases by their cognate response regulator determines cell fate. *Cell* **133**: 452-461.

Paul, R., Weiser, S., Amiot, N.C., Chan, C., Schirmer, T., Giese, B., and Jenal, U. (2004) Cell cycle-dependent dynamic localization of a bacterial response regulator with a novel di-guanylate cyclase output domain. *Genes Dev* **18**: 715-727.

Paulsen, I.T., Seshadri, R., Nelson, K.E., Eisen, J.A., Heidelberg, J.F., Read, T.D., Dodson, R.J., Umayam, L., Brinkac, L.M., Beanan, M.J., Daugherty, S.C., Deboy, R.T., Durkin, A.S., Kolonay, J.F., Madupu, R., Nelson, W.C., Ayodeji, B., Kraul, M., Shetty, J., Malek, J., Van Aken, S.E., Riedmuller, S., Tettelin, H., Gill, S.R., White, O., Salzberg, S.L., Hoover, D.L., Lindler, L.E., Halling, S.M., Boyle, S.M., and Fraser, C.M. (2002) The Brucella suis genome reveals fundamental similarities between animal and plant pathogens and symbionts. *Proc Natl Acad Sci U S A* **99**: 13148-13153.

Petersen, E., Chaudhuri, P., Gourley, C., Harms, J., and Splitter, G. (2011) Brucella melitensis cyclic di-GMP phosphodiesterase BpdA controls expression of flagellar genes. *J Bacteriol* **193**: 5683-5691.

Radkov, A.D., Hsu, Y.P., Booher, G., and VanNieuwenhze, M.S. (2018) Imaging Bacterial Cell Wall Biosynthesis. *Annu Rev Biochem* **87**: 991-1014.

Rao, F., Yang, Y., Qi, Y., and Liang, Z.X. (2008) Catalytic mechanism of cyclic di-GMP-specific phosphodiesterase: a study of the EAL domain-containing RocR from Pseudomonas aeruginosa. *J Bacteriol* **190**: 3622-3631.

Rosen, D.A., Twentyman, J., and Hunstad, D.A. (2018) High Levels of Cyclic Di-GMP in Klebsiella pneumoniae Attenuate Virulence in the Lung. *Infect Immun* **86**.

Ryan, R.P., Fouhy, Y., Lucey, J.F., Crossman, L.C., Spiro, S., He, Y.W., Zhang, L.H., Heeb, S., Camara, M., Williams, P., and Dow, J.M. (2006) Cell-cell signaling in Xanthomonas campestris involves an HD-GYP domain protein that functions in cyclic di-GMP turnover. *Proc Natl Acad Sci U S A* **103**: 6712-6717.

Ryjenkov, D.A., Tarutina, M., Moskvin, O.V., and Gomelsky, M. (2005) Cyclic diguanylate is a ubiquitous signaling molecule in bacteria: insights into biochemistry of the GGDEF protein domain. *J Bacteriol* **187**: 1792-1798.

Schaper, S., Krol, E., Skotnicka, D., Kaever, V., Hilker, R., Sogaard-Andersen, L., and Becker, A. (2016) Cyclic Di-GMP Regulates Multiple Cellular Functions in the Symbiotic Alphaproteobacterium Sinorhizobium meliloti. *J Bacteriol* **198**: 521-535.

Schaper, S., Yau, H.C.L., Krol, E., Skotnicka, D., Heimerl, T., Gray, J., Kaever, V., Sogaard-Andersen, L., Vollmer, W., and Becker, A. (2018) Seven-transmembrane receptor protein RgsP and cell wall-binding protein RgsM promote unipolar growth in Rhizobiales. *PLoS Genet* **14**: e1007594.

Schmidt, A.J., Ryjenkov, D.A., and Gomelsky, M. (2005) The ubiquitous protein domain EAL is a cyclic diguanylate-specific phosphodiesterase: enzymatically active and inactive EAL domains. *J Bacteriol* **187**: 4774-4781.

Schneider, C.A., Rasband, W.S., and Eliceiri, K.W. (2012) NIH Image to ImageJ: 25 years of image analysis. *Nat Methods* **9**: 671-675.

Schultz, J., Milpetz, F., Bork, P., and Ponting, C.P. (1998) SMART, a simple modular architecture research tool: identification of signaling domains. *Proc Natl Acad Sci U S A* **95**: 5857-5864.

Simon, R., Priefer, U., and Pühler, A. (1983) A Broad Host Range Mobilization System for In Vivo Genetic Engineering: Transposon Mutagenesis in Gram Negative Bacteria. *Bio/Technology* **1**: 784-791.

Sohn, A.H., Probert, W.S., Glaser, C.A., Gupta, N., Bollen, A.W., Wong, J.D., Grace, E.M., and McDonald, W.C. (2003) Human neurobrucellosis with intracerebral granuloma caused by a marine mammal Brucella spp. *Emerg Infect Dis* **9**: 485-488.

Starkey, M., Hickman, J.H., Ma, L., Zhang, N., De Long, S., Hinz, A., Palacios, S., Manoil, C., Kirisits, M.J., Starner, T.D., Wozniak, D.J., Harwood, C.S., and Parsek, M.R. (2009) Pseudomonas aeruginosa rugose small-colony variants have adaptations that likely promote persistence in the cystic fibrosis lung. *J Bacteriol* **191**: 3492-3503.

Sternon, J.F., Godessart, P., Goncalves de Freitas, R., Van der Henst, M., Poncin, K., Francis, N., Willemart, K., Christen, M., Christen, B., Letesson, J.J., and De Bolle, X. (2018) Transposon Sequencing of Brucella abortus Uncovers Essential Genes for Growth In Vitro and Inside Macrophages. *Infect Immun* **86**.

Suarez-Esquivel, M., Baker, K.S., Ruiz-Villalobos, N., Hernandez-Mora, G., Barquero-Calvo, E., Gonzalez-Barrientos, R., Castillo-Zeledon, A., Jimenez-Rojas, C., Chacon-Diaz, C., Cloeckaert, A., Chaves-Olarte, E., Thomson, N.R., Moreno, E., and Guzman-Verri, C. (2017) Brucella Genetic Variability in Wildlife Marine Mammals Populations Relates to Host Preference and Ocean Distribution. *Genome Biol Evol* **9**: 1901-1912.

Suarez-Esquivel, M., Chaves-Olarte, E., Moreno, E., and Guzman-Verri, C. (2020) Brucella Genomics: Macro and Micro Evolution. *Int J Mol Sci* **21**.

Teyssier, C., Marchandin, H., Jean-Pierre, H., Diego, I., Darbas, H., Jeannot, J.L., Gouby, A., and Jumas-Bilak, E. (2005) Molecular and phenotypic features for identification of the opportunistic pathogens Ochrobactrum spp. *J Med Microbiol* **54**: 945-953.

Tsolis, R.M., Seshadri, R., Santos, R.L., Sangari, F.J., Lobo, J.M., de Jong, M.F., Ren, Q., Myers, G., Brinkac, L.M., Nelson, W.C., Deboy, R.T., Angiuoli, S., Khouri, H., Dimitrov, G., Robinson, J.R., Mulligan, S., Walker, R.L., Elzer, P.E., Hassan, K.A., and Paulsen, I.T. (2009) Genome degradation in Brucella ovis corresponds with narrowing of its host range and tissue tropism. *PLoS One* **4**: e5519.

Vassen, V., Valotteau, C., Feuillie, C., Formosa-Dague, C., Dufrene, Y.F., and De Bolle, X. (2019) Localized incorporation of outer membrane components in the pathogen Brucella abortus. *EMBO J* **38**.

Verger, J.-M., Grimont, F., Gromon, P.A.D., and Grayon, M. (1985) *Brucella*, a monospecific genus as shown by deoxyribonucleic acid hybridization. *International Journal of systematic and evolutionary microbiology* **34**: 292-295.

Wattam, A.R., Foster, J.T., Mane, S.P., Beckstrom-Sternberg, S.M., Beckstrom-Sternberg, J.M., Dickerman, A.W., Keim, P., Pearson, T., Shukla, M., Ward, D.V., Williams, K.P., Sobral, B.W., Tsolis, R.M., Whatmore, A.M., and O'Callaghan, D. (2014) Comparative phylogenomics and evolution of the Brucellae reveal a path to virulence. *J Bacteriol* **196**: 920-930.

Wattam, A.R., Williams, K.P., Snyder, E.E., Almeida, N.F., Jr., Shukla, M., Dickerman, A.W., Crasta, O.R., Kenyon, R., Lu, J., Shallom, J.M., Yoo, H., Ficht, T.A., Tsolis, R.M., Munk, C., Tapia, R., Han, C.S., Detter, J.C., Bruce, D., Brettin, T.S., Sobral, B.W., Boyle, S.M., and Setubal, J.C. (2009) Analysis of ten Brucella genomes reveals evidence for horizontal gene transfer despite a preferred intracellular lifestyle. *J Bacteriol* **191**: 3569-3579.

Williams, M.A., Aliashkevich, A., Krol, E., Kuru, E., Bouchier, J.M., Rittichier, J., Brun, Y.V., VanNieuwenhze, M.S., Becker, A., Cava, F., and Brown, P.J.B. (2021) Unipolar Peptidoglycan Synthesis in the Rhizobiales Requires an Essential Class A Penicillin-Binding Protein. *mBio*: e0234621.

Figures legends

Figure 1: **Distribution of diguanylate cyclases (DGC) and phosphodiesterases (PDE) in *Brucella* species**.

Homology analysis displaying the conservation of GGDEF (purple squares) or EAL (green circles) domains containing proteins among *Brucellae* and their ancestor *Ochrobactrum anthropi*. The absence of symbol indicates the absence of an ortholog. Predicted pseudogenes in *B. abortus* 2308 are indicated in italic. Figure is adapted from Wattam *et al*. (Wattam *et al.*, 2014).

Figure 2: **PdeA is required for the rod-shape morphology of *B. abortus*.**

(A) Colony morphologies on TSB agar plates. Strains were plated on TSB agar plates and imaged after 4 days of incubation at 37°C. Deletion of *pdeA* leads to small colony formation. Pictures are from one experiment representative of at least 3 independent experiments. Scale bar, 0.5cm.

(B) Phase contrast micrographs of *B. abortus* 544 pMR10 (WT), Δ*pdeA* pMR10 (Δ*pdeA*) mutant and complemented strain (Δ*pdeA* pMR10::*pdeA*) grown until exponential phase in TSB at 37°C. Scale bar, 2 μm.

(C-E) Violin plot of width to length ratio (w/L) (C), lengths (D), and widths (E). The Δ*pdeA* mutant is significantly rounder, shorter and wider than the WT strain, respectively (****, $p < 0.0001$, in one-way analysis of variance). For each violin plot graphs, the totality of measured bacteria from three independent experiments is shown. Statistics were calculated on the three independent medians. Medians (hatched bars) and quartile (dot lines) are indicated.

Figure 3: **The role of PdeA in morphology is not related to its phosphodiesterase activity.**

(A) Colony morphologies on TSB agar plates. Strains were plated on TSB agar plates and imaged after 4 days of incubation at 37°C. PdeA carrying a point mutation in its catalytic site grows as the WT strain. Pictures are from one experiment representative of at least 3 independent experiments. Scale bar: 0.5 cm.

(B, E) Phase contrast micrographs of *B. abortus* WT and the catalytic mutants grown until exponential phase growth in TSB at 37°C. Scale bar, 2 μm.

(C-D; F-G) Violin plot of bacterial lengths (C and F) and widths (D and G). Bacteria from 3 independent experiments are plotted. Numbers of measured bacteria, average length, width and w/L ratio are provided in table S1D. Medians (hatched bars) and quartile (dot lines) are indicated.

Figure 4: **Asymmetric growth is maintained in the Δ*pdeA* mutant.**

(A) Microscopic observations of WT strain (upper panels) and Δ*pdeA* mutant (bottom panels). Scale bar, 1 μm

(B) Demographic representation of eFluor labelling from (A). Bacteria were sorted by their length and oriented with eFluor signal (representing the old pole) at the top of the demograph.

(C) Demographic representation of HADA labelled bacteria from (A). Bacteria were sorted by their length and oriented with eFluor signal (representing the old pole) at the top of the demograph. The intensity of purple and cyan corresponds to the normalized fluorescence intensity (NFI). Demograph were aligned on the center of the bacteria.

(D) Quantification of the PG insertion sites from (A). The graph shows the mean of three individual experiments, n_{WT} = 1115 (black bars) bacteria and n_{mutant} = 939 (white bars). GP, Growing Pole; M, Midcell; C, Constriction site (****, $p<0.0001$, **, $p<0.01$, in an unpaired t-test). Only statistically significant differences are highlighted.

(E) Bacterial area. Shown is the total number of considered bacteria from 3 independent experiments. Statistical analysis was performed on the three individual medians.

(F) Percentage of HADA labelled area per bacteria. Main graph is the distribution of all measured bacteria from 3 independent experiments, n_{WT} = 2162 bacteria, n_{mutant} = 784. Insert represents the individual measured medians and the mean of the three medians (bar) (**, $p<0.01$, in an unpaired t-test).

Figure 5: **PdeA is not required for the positioning of known polar proteins.**

(A-C, left panels) Microscopic observations of WT strain (upper pictures) and Δ*pdeA* mutant (bottom pictures) expressing PdhS-YFP (A), FumC-YFP (B) or AidB-YFP (C) Scale bar, 1 μm.

(A-C, center panels) Demographic representations of the fluorescence intensity for PdhS (A), FumC (B) or AidB (C) in the WT strain (top demograph) and the $\Delta pdeA$ mutant strain (bottom demograph). Bacteria were sorted by their lengths and oriented with eFluor (old pole) at the top of the demographs. A representative experiment out of three individual biological replicates is shown (A, n_{WT} = 200, n_{mutant} = 138; B, n_{WT} = 434, n_{mutant} = 198; C, n_{WT} = 90, n_{mutant} = 48). Replicates are provided on Fig S11.

(A-C, right panels) Percentage of bacteria for each localization of PdhS, FumC and AidB in the WT strain strain (black bar) and the $\Delta pdeA$ mutant (white bar). The graph represents the mean of three biological replicates. GP, Growing Pole; M, Midcell; C, Constriction site, O, Old pole, B, Bipolar (ns, non-significant, **, $p<0.01$, ***, $p<0.001$, ****, $p<0.0001$, in a two-way anova). Only statistically significant differences are highlighted.

Figure 6: **PdeA localizes at the growing zones.**

(A, D) Fluorescence microscopy images of *B. abortus* 544 expressing *pdeA-mCherry pdhS-yfp* (A) or expressing *pdeA-mCherry aidB-yfp* (D). Scale bar, 1 μm.
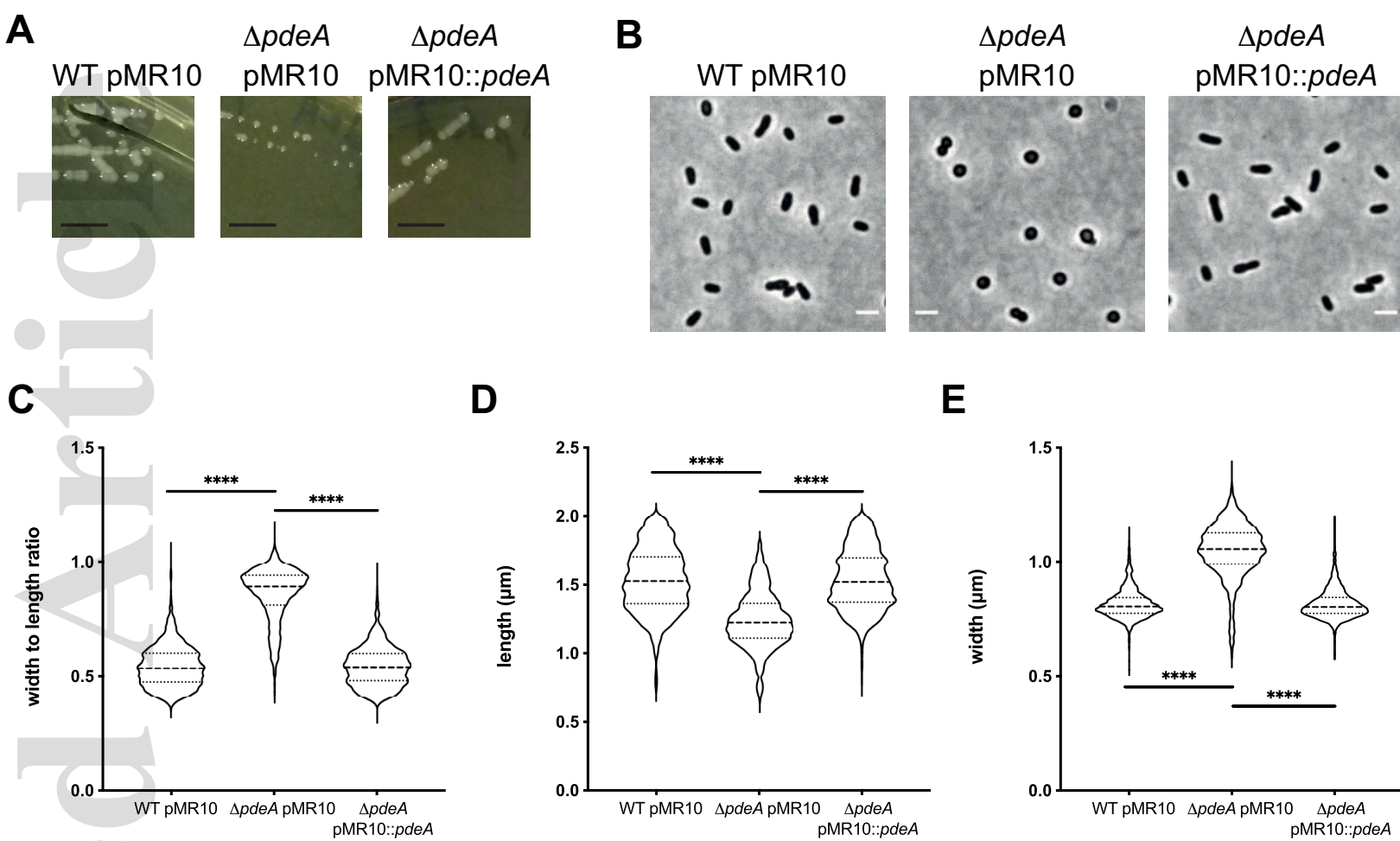
(B, C, E, F) Bacteria were sorted by their lengths and oriented with PdhS at the top of the demographs (B, C, n = 546 bacteria) or AidB at the bottom of the demographs (F, G, n = 141 bacteria). A representative experiment out of three individual biological replicates is shown. Replicates are shown in Fig S12.

(G, H) Quantification of fluorescence intensity of *B. abortus* 544 expressing *pdeA-mCherry pdhS-yfp* (G) or expressing *pdeA-mCherry aidB-yfp* (H). Graphs display the mean percentages from three individual experiments.
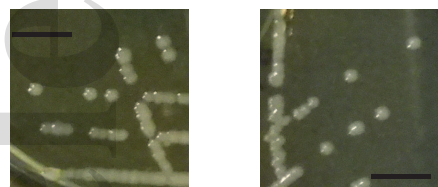
Figure 7: **PdeA is required for optimal organs colonization.**

Time course colonization of lung (A) and spleen (B) at 48 h, 5, 12 and 28 d following intranasal infection of C57BL/6 mice with 2.10^4 WT strain (black circles), $\Delta pdeA$ strain (white triangles) and the complemented strain (grey triangles). A representative experiment out of two is shown. Replicate is shown in Fig S13. Detection threshold is 10 CFU. Red bars represent median values (ns, non-significant, *, $p<0.05$, **, $p<0.01$, ***, $p<0.001$, ****, $p<0.0001$, in a two-way anova with Bonferoni posttest). Data were obtained using 7 or 8 mice per group.

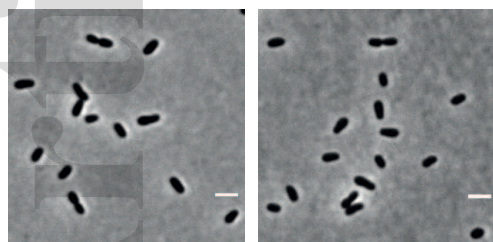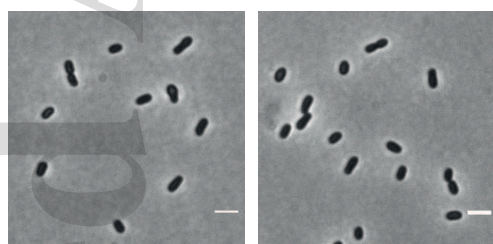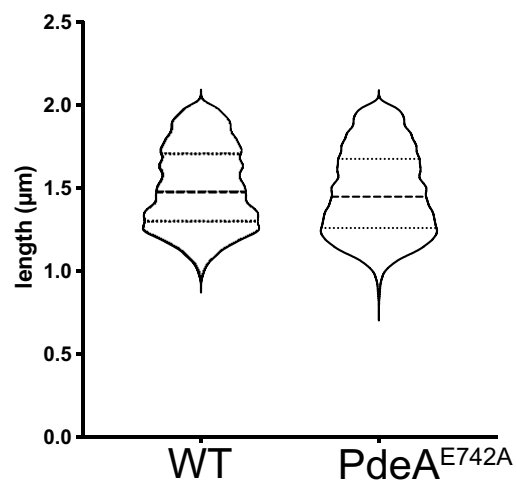mmi_14833_f1.eps

A

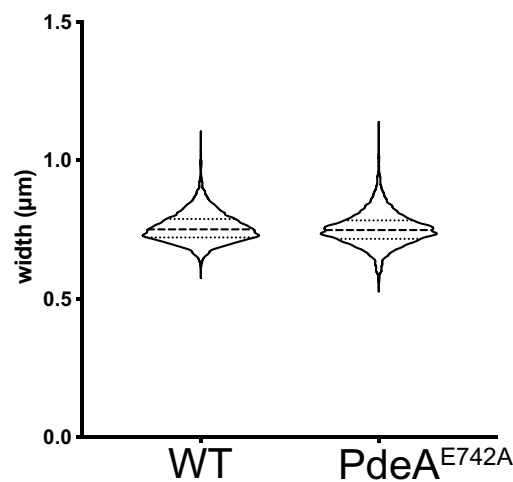WT pMR10 | Δ*pdeA* pMR10 | Δ*pdeA* pMR10::*pdeA*

B

WT pMR10 | Δ*pdeA* pMR10 | Δ*pdeA* pMR10::*pdeA*

C

width to length ratio

****   ****

WT pMR10   Δ*pdeA* pMR10   Δ*pdeA* pMR10::*pdeA*

D

length (µm)

****   ****

WT pMR10   Δ*pdeA* pMR10   Δ*pdeA* pMR10::*pdeA*

E

width (µm)

****   ****

WT pMR10   Δ*pdeA* pMR10   Δ*pdeA* pMR10::*pdeA*
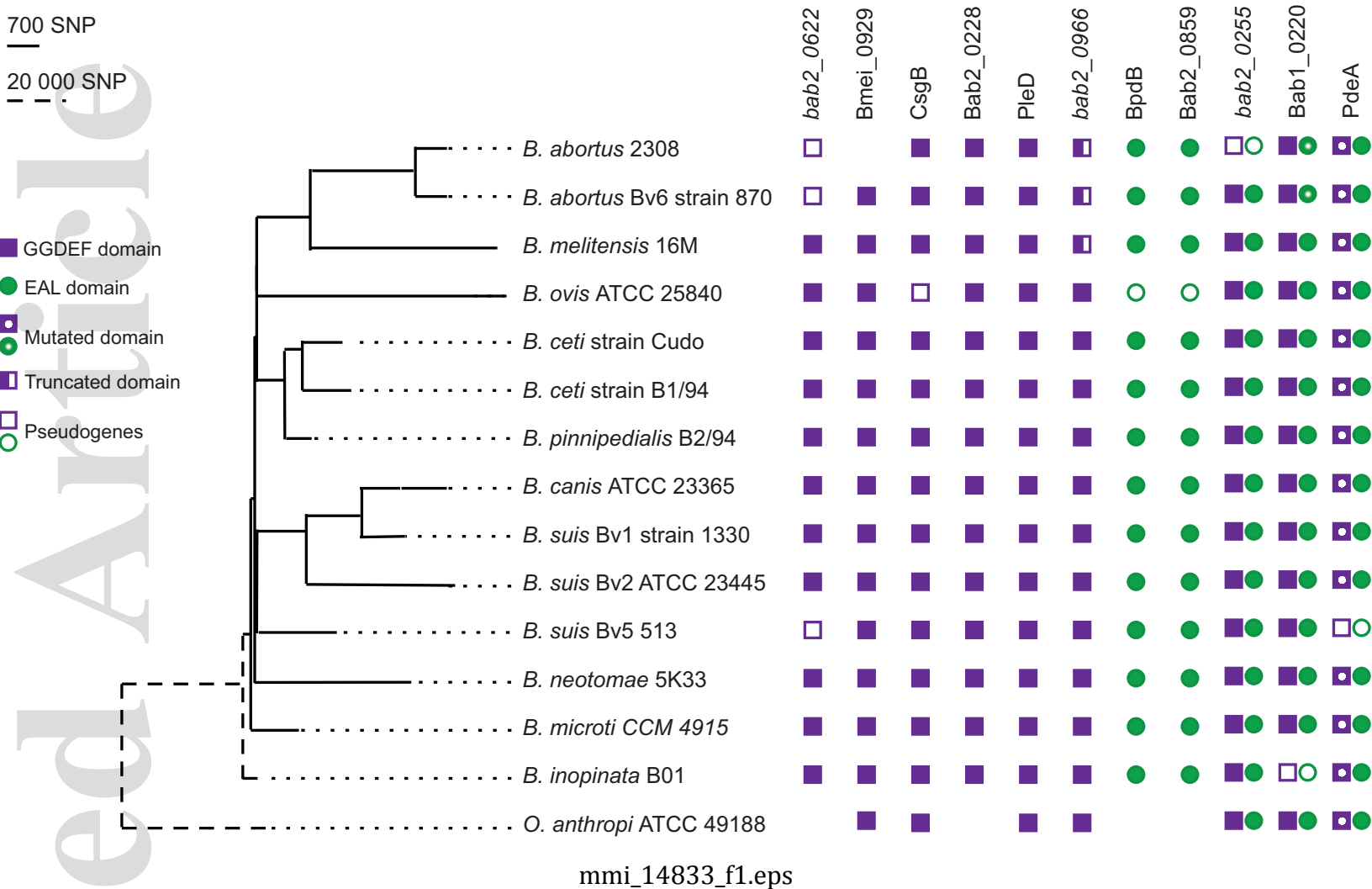
mmi_14833_f2.eps

A

WT

PdeA^E742A

B

WT

PdeA^E742A

E

WT

Δ*B59*
PdeA^E742A

C

D

F

G
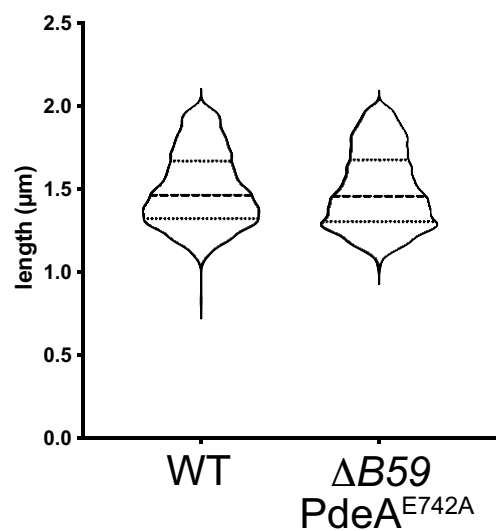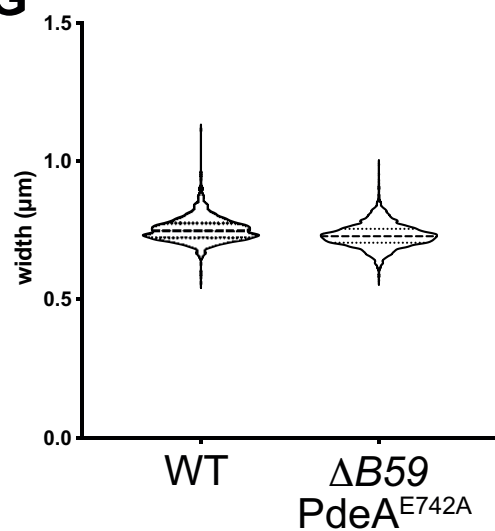
mmi_14833_f3.eps

mmi_14833_f4.eps

mmi_14833_f5.eps

A

Phase | PdhS-YFP
       | PdeA-mCherry

B PdhS-YFP
NFI — Position — Cells sorted by length

C PdeA-mCherry
NFI — Position — Cells sorted by length

D

AidB-YFP
PdeA-mCherry | Merge

E AidB-YFP
NFI — Position — Cells sorted by length

F PdeA-mCherry
NFI — Position — Cells sorted by length

G

% of bacteria / localization

- Growing pole
- Constriction Site
- Midcell
- Others

H

% of bacteria / localization

- Both Growing Pole
- Both Constriction Site
- AidB Midcell or Constriction site / PdeA Polar
- Others

mmi_14833_f6.eps

A

B